Journal of Medicinal Chemistry

Article

pubs.acs.org/jmc

New Inhibitors of Angiogenesis with Antitumor Activity in Vivo

Nagore I. Marín-Ramos,[†,‡,◆] Dulce Alonso,[†,◆] Silvia Ortega-Gutiérrez,[†] Francisco J. Ortega-Nogales,[†] Moisés Balabasquer,[†] Henar Vázquez-Villa,[†] Clara Andradas,[§,∥] Sandra Blasco-Benito,[§,∥] Eduardo Pérez-Gómez,[§,∥] Ángeles Canales,[†] Jesús Jiménez-Barbero,[⊥,¶] Ana Marquina,[#] Jaime Moscoso del Prado,[#] Cristina Sánchez,[§,∥] Mar Martín-Fontecha,*[,†] and María L. López-Rodríguez*[,†]

[†]Departamento de Química Orgánica I, Facultad de Ciencias Químicas, [§]Departamento de Bioquímica y Biología Molecular I, Facultad de Ciencias Biológicas, Universidad Complutense de Madrid, E-28040 Madrid, Spain

[‡]CEI Campus Moncloa, UCM-UPM and CSIC, E-28040 Madrid, Spain

[∥]Instituto de Investigación Hospital 12 de Octubre, E-28041 Madrid, Spain

[⊥]CIC bioGUNE, Parque Tecnológico de Bizkaia, Edif. 801A, 48160 Derio, Spain

[¶]Ikerbasque, Basque Foundation for Science, 48013 Bilbao, Spain

[#]Departamento de Investigación, Italfarmaco S.A., Calle de San Rafael, 3, E-28108 Alcobendas, Madrid, Spain

Supporting Information

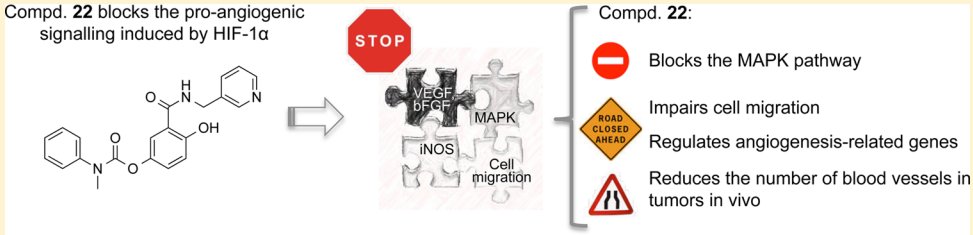

ABSTRACT: Angiogenesis is a requirement for the sustained growth and proliferation of solid tumors, and the development of new compounds that induce a sustained inhibition of the proangiogenic signaling generated by tumor hypoxia still remains as an important unmet need. In this work, we describe a new antiangiogenic compound (**22**) that inhibits proangiogenic signaling under hypoxic conditions in breast cancer cells. Compound **22** blocks the MAPK pathway, impairs cellular migration under hypoxic conditions, and regulates a set of genes related to angiogenesis. These responses are mediated by HIF-1α, since the effects of compound **22** mostly disappear when its expression is knocked-down. Furthermore, administration of compound **22** in a xenograft model of breast cancer produced tumor growth reductions ranging from 46 to 55% in 38% of the treated animals without causing any toxic side effects. Importantly, in the responding tumors, a significant reduction in the number of blood vessels was observed, further supporting the mechanism of action of the compound. These findings provide a rationale for the development of new antiangiogenic compounds that could eventually lead to new drugs suitable for the treatment of some types of tumors either alone or in combination with other agents.

INTRODUCTION

Angiogenesis, the process of new blood vessel formation, is a requirement for the sustained growth and proliferation of solid tumors. Accordingly, the search for inhibitors of this process has become a leading line of investigation in anticancer research, and it has translated into several drugs in the market that have clearly improved outcomes in patients with different tumor types and metastatic disease. Among these agents, Bevacizumab (Avastin, Genentech Ltd.) was the first antiangiogenic drug approved by the FDA in 2004.[1] Bevacizumab is a monoclonal antibody that targets vascular endothelial growth factor (VEGF, also known as VEGFA) and hinders its from binding to its corresponding receptor, thus blocking its signaling. Initially considered a first-line treatment for metastatic colorectal cancer, it is also prescribed for the treatment of other types of cancer, and its development still stands out as one of the landmark achievements of anticancer research.[2,3] Although today other drugs with similar mechanisms of action have progressed into the clinic,[3−5] several limitations exist, such as the lack of efficacy in some patients, the appearance of adverse effects, and drug resistance. Among them, this last one is perhaps the most important efficacy-limiting factor of current antiangiogenic therapies. It has been suggested that when VEGF signaling is pharmacologically blocked other proangiogenic factors take over its signaling, thereby supporting tumor angiogenesis.[3,6,7] Amid these compensatory angiogenesis pathways, fibroblast growth factor

Received: December 12, 2014
Published: April 23, 2015

DOI: 10.1021/jm5019252
J. Med. Chem. 2015, 58, 3757−3766

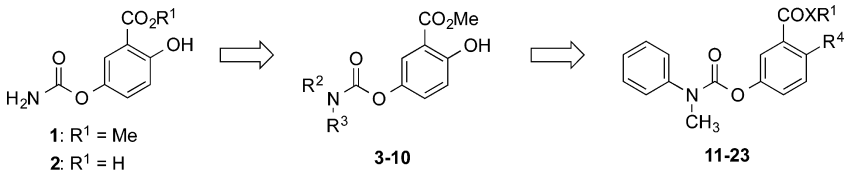

Figure 1. Exploration of the scaffold of the initial hit **1**.

Scheme 1[a]

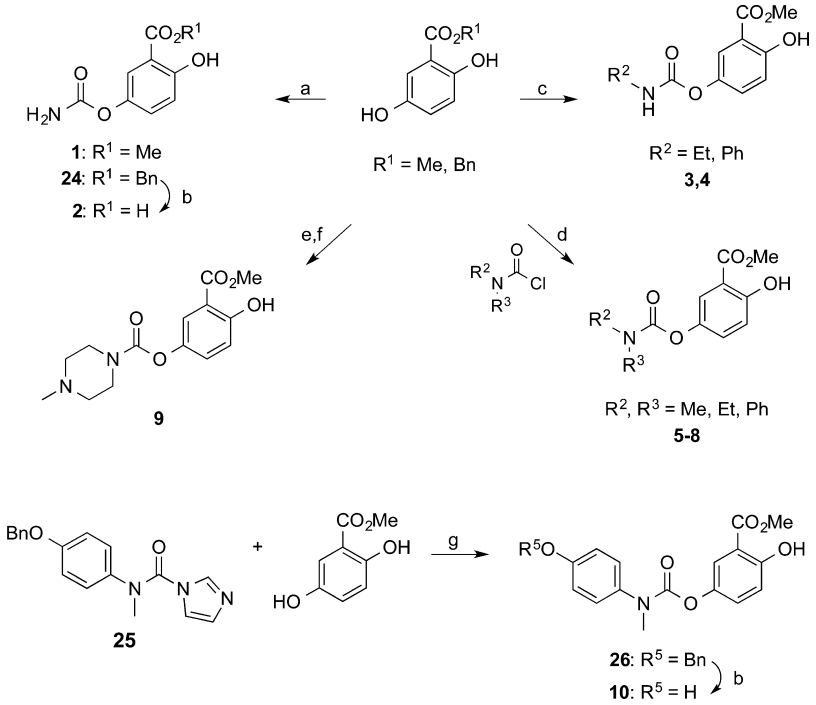

[a]Reagents and conditions: (a) CSI, CH_2Cl_2, rt, o/n, 30−34%; (b) H_2, Pd(C), EtOH, rt, 3 h, 100%; (c) R^2NCO, DIEA, THF, rt, 16 h, 70−71%; (d) NaH, CH_3CN, rt, 3 h, 14−64%; (e) 4-nitrophenylchloroformate, DABCO, CH_2Cl_2, rt, 5 h, 40%; (f) 1-methylpiperazine, DIEA, CH_2Cl_2, 0 °C to rt, 3 h, 67%; (g) CH_3I, CH_3CN, rt, 24 h, 36%.

(FGF) seems to play an integral role in the resistance to anti-VEGF therapy, and different studies have suggested a critical role of FGF signaling in clinical tumor progression.[8−10] Although targeting FGF signaling has lagged behind that of other receptor tyrosine kinases, there is now substantial evidence for the importance of FGF signaling in the pathogenesis of diverse tumor types. Hence, the development of compounds that inhibit the FGF pathway is receiving much attention, although they are still early in development.[11−13] Among the different FGFs, FGF-2, also known as basic FGF (bFGF), has been functionally implicated in tumor angiogenesis and it is an important target of antiangiogenic therapies.[8,11,13,14] Notwithstanding the importance of blocking angiogenesis for antitumor therapies, it has been shown that prolonged antiangiogenic treatments eventually lead not only to drug resistance but also to enhanced tumor migration and metastasis.[15−17] The main reason for this is that an antiangiogenic compound will eventually generate a hypoxic microenvironment, which turns on proangiogenic signaling, increasing the levels of factors that promote the acquisition of an invasive and metastatic tumor phenotype such as nitric oxide (NO), VEGF, and FGF. In addition, the same cells often express the cognate membrane receptors for these factors, resulting in autocrine signaling.[18] Accordingly, the development of new antitumor compounds that simultaneously block angiogenesis and induce a sustained inhibition of the proangiogenic signaling generated by hypoxia currently remains an important unmet need, as these agents should be more effective drugs than the ones currently in the clinic and should lack the associated more aggressive recurrence with metastasis and drug resistance.

In this context, we have started a project aimed at the identification of new small molecules able to block FGF signaling using our in-house library and a bFGF-induced cell proliferation assay as the primary screen. After identification of an initial hit, the subsequent hit-to-lead process has allowed us to develop a new inhibitor of angiogenesis (compound **22**) that impairs proangiogenic signaling under hypoxic conditions in breast cancer cells, blocks the mitogen-activated protein kinase (MAPK) pathway, inhibits cellular migration, and regulates a set of genes related to angiogenesis. Furthermore, administration of compound **22** in a breast cancer xenograft model significantly decreased the number of blood vessels in tumors and produced tumor growth reductions from 46 to 55% in 38% of the treated animals without causing any toxic side effects.

RESULTS AND DISCUSSION

Hit Identification and Hit-to-Lead Process. Selected representative compounds from our in-house library were screened in a bFGF-induced cell proliferation assay using

DOI: 10.1021/jm5019252
J. Med. Chem. 2015, 58, 3757−3766

human umbilical vein endothelial cells (HUVECs) in order to identify a chemically tractable hit with drug-like properties that could be amenable to further optimization. From this screening, carbamate **1** emerged as an initial hit with an IC_{50} value of 317 μM. We started the exploration of this scaffold (Figure 1) by introducing substituents in the carbamate group and keeping the methyl ester moiety constant (as its removal led to complete inactivity of the corresponding carboxylic acid, derivative **2**, IC_{50} > 500 μM) as well as the phenolic hydroxyl group (compounds **3**–**10**). Target compounds were synthesized as depicted in Scheme 1. Reaction of methyl or benzyl 2,5-dihydroxybenzoate with chlorosulfonylisocyanate (CSI) followed by benzyl ester cleavage of intermediate **24** yielded carbamates **1** and **2**, respectively. N-Monosubstituted carbamates **3** and **4** were obtained by addition of methyl 2,5-dihydroxybenzoate to ethyl and phenyl isocyanate in the presence of *N*,*N*-diisopropylethylamine (DIEA) as a base, whereas reaction of methyl 2,5-hydroxybenzoate with the corresponding carbamoyl chloride afforded disubstituted carbamates **5**–**8**. Piperazine derivative **9** was synthesized by nucleophilic substitution of 4-nitrophenylchloroformate with methyl 2,5-dihydroxybenzoate followed by treatment of the resultant carbonate with 1-methylpiperazine. Alternatively, acylation of methyl 2,5-dihydroxybenzoate with carbonylimidazol derivative **25** gave intermediate **26**, which afforded final compound **10** by benzyl ether deprotection under palladium-catalyzed hydrogenation. Carbamates **2**–**10** were screened for activity in the bFGF-induced proliferation assay (Table 1).

Table 1. Inhibition of bFGF-Induced Cell Proliferation of Human Umbilical Vein Endothelial Cells (HUVECs) by Compounds 1–10

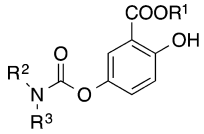

compd	R^1	R^2	R^3	IC_{50} (μM)[a]
1	Me	H	H	317
2	H	H	H	>500
3	Me	Et	H	17
4	Me	Ph	H	165
5	Me	Me	Me	>500
6	Me	Et	Et	>500
7	Me	Ph	Me	48
8	Me	Ph	Ph	35
9	Me	$(CH_2)_2NCH_3(CH_2)_2$		>500
10	Me	*p*-hydroxyphenyl	Me	96

[a]IC_{50} values are the means from two to three independent experiments performed in triplicate. In all cases, the SEM is within 10% of the mean value.

From the obtained results, the main conclusion is that the replacement of a hydrogen of the carbamate group by an ethyl or phenyl group gave active compounds (**3** and **4**), whereas disubstitution of the carbamate with alkyl chains is detrimental for activity (compounds **5**, **6**, and **9**, IC_{50} > 500 μM). However, when one or both substituents are aromatic rings, the antiproliferative activity is restored (**7**, **8**, and **10**). Among this first series of compounds, carbamates **3**, **7**, and **8** deserve special attention because they show the highest potency in inhibiting cell proliferation, with IC_{50} values of 17, 48, and 35 μM, respectively. In order to select the best scaffold to continue with the optimization process, we determined some pharmacokinetic parameters (Table 2). Although the most potent derivative, **3**, showed a disappointingly low stability that disqualified it from being a suitable candidate for further optimization, compound **7** showed good properties, especially in terms of aqueous solubility, lipophilicity, permeability, and stability. Therefore, it was selected for further structural exploration focused on whether the phenolic hydroxy group was required for activity and to determine if it was possible to replace the methyl ester group without a significant activity decrease (compounds **11**–**23**; Figure 1). These new derivatives were synthesized as depicted in Scheme 2. Disubstituted carbamates **11**, **12**, and **14**–**18** were prepared by reaction of the corresponding 5-hydroxybenzoates with *N*-methyl-*N*-phenylcarbamoyl chloride. Methyl ester **7** was transformed into amide **13** by reaction with methylamine. Finally, phenyl methyl carbamates **19**–**23** were obtained by condensation of carboxylic acid **28** with the corresponding alcohol or amine in the presence of 1-ethyl-3-(3-(dimethylamino)propyl)carbodiimide (EDC) as a coupling reagent. All of these new compounds were screened for activity (Table 3). Our results suggest that the phenolic hydroxy group is essential for activity, since both its methylation (compound **11**) or removal (derivative **12**) led to important decreases in activity (IC_{50} (**7**) = 48 μM vs IC_{50} (**11**) = 118 μM and IC_{50} (**12**) = 290 μM; Table 3). Accordingly, the phenolic hydroxy group was kept in carbamates **13**–**23**, and different esters and amides were introduced in an attempt to replace the initial methyl ester group. Our first attempt was to prepare amide **13**, an analogue of **7**, but this change led to a decrease in activity (IC_{50} value for **7** was 48 μM, whereas amide **13** showed an IC_{50} value of 67 μM; Table 3). This result suggested that the substitution of the ester by an amide would probably involve some reduction in biological activity, so we first kept the ester bond but replaced the methyl group by other aliphatic and (hetero)aromatic groups in search of better activities. In this case, we could later substitute the ester by an amide group and still maintain good activity values. With this idea in mind, esters **14**–**20** were prepared. Among them, the best results in terms of IC_{50} values were obtained for benzyl and

Table 2. Pharmacokinetic Properties of Compounds 3, 7, 8, 21, and 22[a]

property	compound 3	7	8	21	22
aqueous solubility (PBS, pH 7.4, μM)	ND	103.5	5.8	35	175.7
partition coefficient (LogD, *n*-octanol/PBS, pH 7.4)	ND	3.13	4.46	4.19	2.95
chemical stability pH 7.4 (remaining compound, %)	ND	67	24	93	108
A–B permeability (TC7, pH 6.5/7.4, 10^{-6} cm/s)	ND	46.1	7.9	35.1	53.5
human plasma stability (remaining compound, %)	<5	94	105	87	111
mouse plasma stability (remaining compound, %)	<5	83	89	78	99

[a]Data are expressed as the mean from two independent experiments performed in duplicate. The SEM in all cases is within 10% of the mean value. ND, not determined. For stability studies, the percentage of the remaining compound after 1 h is given.

DOI: 10.1021/jm5019252
J. Med. Chem. 2015, 58, 3757–3766

Scheme 2[a]

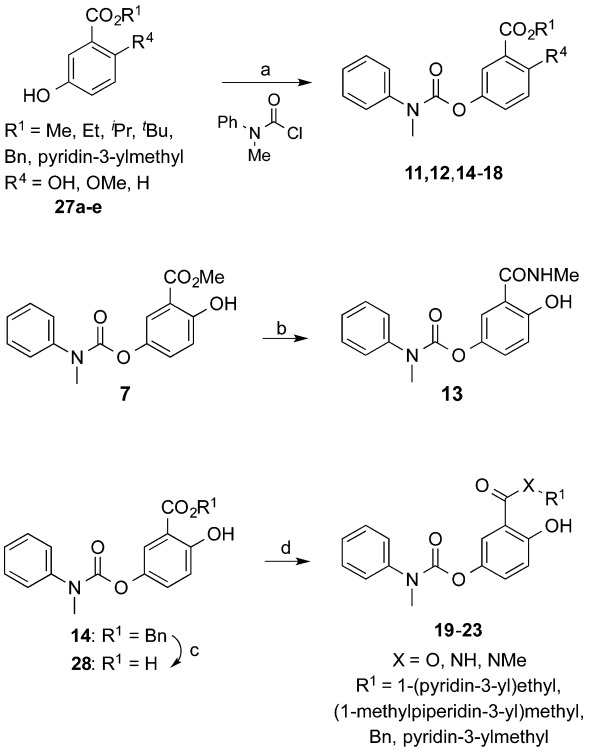

[a]Reagents and conditions: (a) NaH, CH_3CN, rt, 3 h, 14–64%; (b) CH_3NH_2, CH_3OH, 0 °C to rt, 3 h, 76%; (c) H_2, Pd(C), EtOH, rt, 3 h, 100%; (d) R^1OH, R^1NH_2, or R^1NHMe, EDC, DMAP, DMF, 0 °C to rt, 16 h, 27–64%.

3-methylpyridinyl groups as R^1 substituents, compounds **14** and **18**, with IC_{50} values of 17 and 16 μM, respectively (Table 3). Hence, these two R^1 groups were selected, and the analogue amides **21–23** were synthesized. The biological activity of these amides was similar to that of the corresponding esters, as shown, for example, by the IC_{50} values of esters **14** and **18** (17 and 16 μM, respectively) when compared with the IC_{50} values of amides **21** and **22** (22 and 14 μM, respectively). Hence, we determined their pharmacokinetic properties in order to select the best candidate to continue with the biological studies. Taking into account all of these data (Table 2), amide **22** showed the best overall profile with the highest solubility (175.7 μM), stability (around 100% under the three assayed conditions), and permeability values. Accordingly, this compound was selected for in-depth characterization.

Compound 22 Inhibits Proangiogenic Signaling in MCF7 Breast Cancer Cells under Hypoxic Conditions. Tumor hypoxia, a common feature of many solid tumors, has been identified as a key driver for angiogenic regulation mechanisms. Hence, we first explored whether compound **22** is able to inhibit the proangiogenic signaling generated by hypoxia in the MCF7 human breast adenocarcinoma cell line that was chosen as a model. Our results show that compound **22** decreases the levels of important proangiogenic factors VEGF and bFGF in hypoxic MCF7 cells (Figure 2A,B). In addition, this derivative also induces a decrease in the NO levels, which runs parallel to a strong inhibition of iNOS expression (Figure 2C,F).

Considering the importance of the enhancement of autocrine signaling under hypoxic conditions, especially in terms of

Table 3. Inhibition of bFGF-Induced Cell Proliferation of Human Umbilical Vein Endothelial Cells (HUVECs) by Compounds 11–23[a]

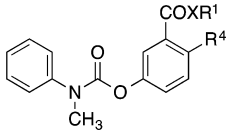

Cpd	X	R^1	R^4	IC_{50} (μM)
7	O	Me	OH	48
11	O	Me	OMe	118
12	O	Me	H	290
13	NH	Me	OH	67
14	O	Bn	OH	17
15	O	Et	OH	28
16	O	Isopropyl	OH	26
17	O	*tert*-Butyl	OH	25
18	O		OH	16
19	O		OH	39
20	O		OH	74
21	NH	Bn	OH	22
22	NH		OH	14
23	N(Me)			90

[a]IC_{50} values are the means from two to three independent experiments performed in triplicate. In all cases, the SEM is within 10% of the mean value.

activation of the corresponding receptors, VEGFR and FGFR, we also assessed whether compound **22** affected their activation. Remarkably, this derivative inhibits the activation of these two receptors, as it decreases their phosphorylated (active) forms (Figure 2D,E).

The main effects of the activation of the FGFR pathway include the induction of proliferation, migration, and antiapoptotic signals. Proliferation enhancement is mainly achieved through activation of the MAPK cascade, whereas the induction of antiapoptotic signals is mediated by activation of the PI3K/AKT pathway.[8,11] This latter cell survival pathway is also reinforced by VEGFR activation.[3] Hence, we explored whether compound **22** was able to suppress the phosphorylation of downstream kinases AKT, MEK, and ERK. As expected, hypoxia activated the AKT and the MEK and ERK signaling pathways, as demonstrated by the increased phosphorylation of these kinases, and, remarkably, incubation of the cells with compound **22** prevented this activation (Figure 3A). Importantly, inhibition of these signaling pathways by compound **22** was accompanied by an impairment in hypoxia-stimulated cell migration (Figure 3B). In order to determine whether the decrease in migration was due to general cytotoxicity, we carried out a similar set of experiments in which cells were incubated with compound **22** for 48 h, after which the compound was removed and then the cells were

DOI: 10.1021/jm5019252
J. Med. Chem. 2015, 58, 3757–3766

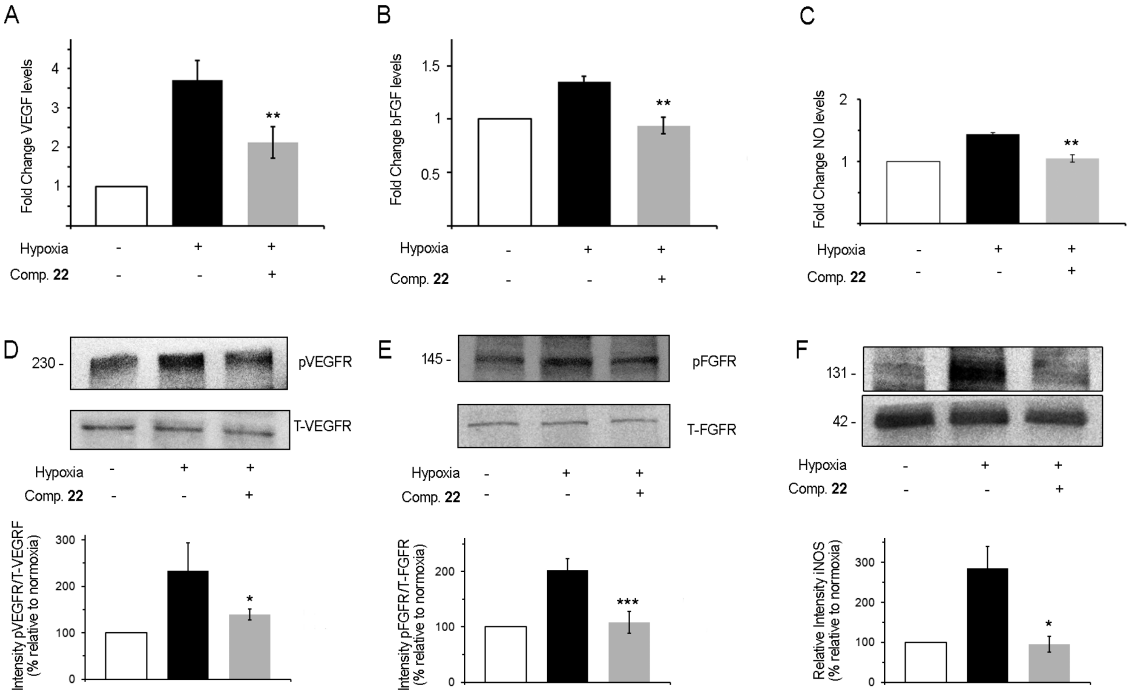

Figure 2. Compound **22** decreases the production of hypoxia-induced proangiogenic factors VEGF, bFGF, and NO and inhibits the activation of their corresponding receptors. Incubation of MCF7 cells with compound **22** (50 μM) under hypoxic conditions significantly reduces the levels of (A) VEGF, (B) bFGF, and (C) NO, decreases the activation of the (D) VEGF and (E) FGF receptors, and decreases (F) iNOS expression (131 kDa band). β-Actin (42 kDa) is shown as a loading control. Data correspond to the average ± SEM of at least three independent experiments, and representative gels are shown. The bar graphs in panels D and E represent the optical density of the immunoreactive phosphorylated protein normalized to the total corresponding protein, which is expressed as the percentage relative to normoxia. The bar graph in panel F represents the optical density of the immunoreactive protein (iNOS) expressed as the percentage relative to normoxia. *, $P < 0.05$; **, $P < 0.01$; ***, $P < 0.001$ (vs hypoxic vehicle-treated cells) (Student's t test).

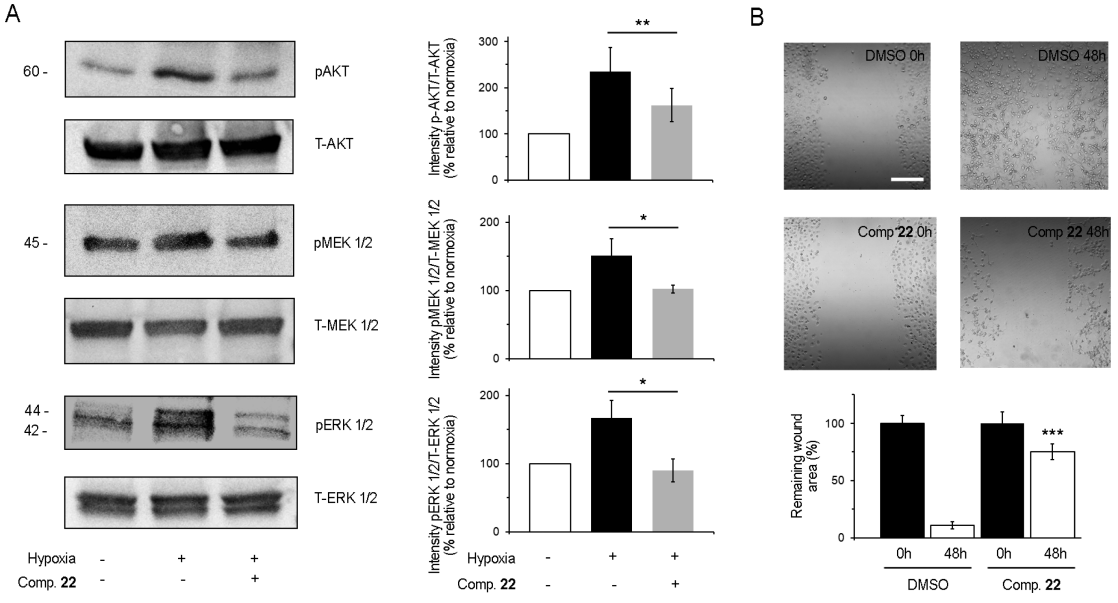

Figure 3. Compound **22** inhibits hypoxia-activated signaling pathways and suppresses cell migration. (A) Representative western blots of phosphorylated (pAKT) and total AKT (T-AKT), phosphorylated MEK1/2 (pMEK1/2) and total MEK1/2 (T-MEK1/2), and phosphorylated ERK1/2 (pERK1/2) and total ERK1/2 (T-ERK1/2). Lysates were obtained from MCF7 cells treated with compound **22** (50 μM) under hypoxic conditions. Data correspond to the average ± SEM of at least three independent experiments. The bar graphs in panel A represent the optical density of the immunoreactive phosphorylated protein normalized to the total corresponding protein, which is expressed as the percentage relative to normoxia. *, $P < 0.05$; **, $P < 0.01$ (Student's t test). (B) In vitro scratches (wounds) were made by scraping confluent cell monolayers with a sterile pipet tip and were visualized by phase contrast microscopy. After 48 h under hypoxic conditions, the remaining wound area was quantified. The bar graph represents the average ± SEM of at least three independent experiments and three different fields. ***, $P < 0.001$ (vs DMSO-treated cells) (Student's t test). Bar, 250 μm.

DOI: 10.1021/jm5019252
J. Med. Chem. 2015, 58, 3757−3766

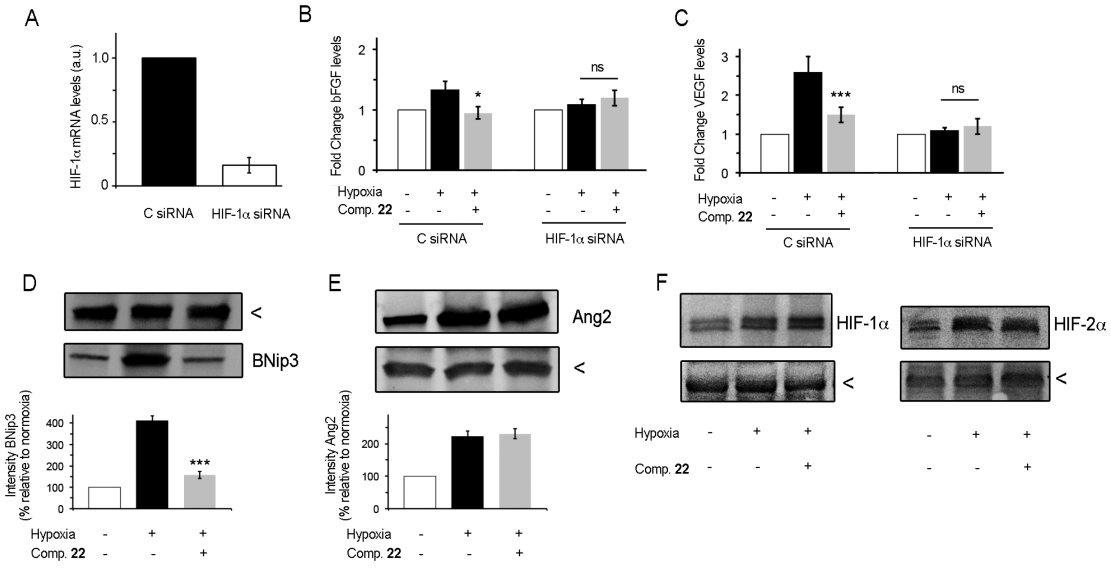

Figure 4. Compound **22** inhibits the production of the hypoxia-induced proangiogenic factors via HIF-1α. (A) HIF-1α mRNA levels after transient transfection of MCF7 cells with a siRNA selectively targeting HIF-1α (HIF-1α siRNA) or with a nontargeted siRNA (C siRNA). Results are expressed in arbitrary units (au). bFGF (B) and VEGF (C) levels in MCF7 cells transiently transfected with the indicated siRNAs under normoxic and hypoxic conditions and in the presence/absence of compound **22**. Representative western blots of (D) BNip3 (22 kDa), (E) Ang2 (65 kDa), and (F) HIF-1α (132 kDa) and HIF-2α (115 kDa). In all cases, actin (42 kDa), marked with an arrowhead, is used as a loading control. Lysates were obtained from MCF7 cells treated with compound **22** (50 μM) under normoxic or hypoxic conditions as indicated. Data correspond to the average ± SEM of at least three independent experiments. The bar graphs in panels D and E represent the optical density of the immunoreactive protein (BNip3 or Ang2, respectively) expressed as the percentage relative to normoxia. *, $P < 0.05$; ***, $P < 0.001$ (vs hypoxic vehicle-treated cells) (Student's t test).

incubated for an additional 48 h. The obtained results show that cells recover their ability to migrate after removal of the compound (Supporting Information Figure S1). In addition, the number of viable cells remains similar to that in the vehicle-treated cells (Supporting Information Figure S1E). Taken together, these data strongly suggest that compound **22** is mainly affecting cell migration and not inducing general cytotoxicity.

Compound 22 Inhibits the Production of Hypoxia-Induced Proangiogenic Signals via Hypoxia-Inducible Factor-1α (HIF-1α). Intratumoral hypoxia is one of the major factors that drive tumor angiogenesis, and hypoxia-driven angiogenesis is primarily mediated by HIF-1α, often considered to be a master regulator of angiogenesis under hypoxia.[19] In addition, in MCF7 breast cancer cells, HIF-1α is the factor that mainly contributes to the expression of genes under hypoxic conditions.[20] Therefore, we analyzed whether HIF-1α was involved in the antiangiogenic response elicited by compound **22**. To this end, we knocked-down HIF-1α using selective small interfering RNAs (siRNAs) (Figure 4A). As shown in Figure 4B,C, hypoxia induced an increase in bFGF and VEGF levels in MCF7 cells transfected with a nontargeted (control) siRNA (C siRNA), and this effect was prevented by compound **22**. Conversely, genetic silencing of HIF-1α abrogated the increase in these two proangiogenic factors upon hypoxia stimulus, and compound **22** did not enhance this effect. These results suggest that the effect of compound **22** on bFGF and VEGF levels is mediated via HIF-1α. To further ascribe the effects of compound **22** to HIF-1α modulation and not to other members of its family, mainly HIF-2α, we selected two proteins, BNip3 and Ang-2, which have been described to be mainly regulated by HIF-1α and HIF-2α, respectively.[21] As expected, and consistent with the literature, hypoxia increased the levels of both proteins, BNip3 and Ang-2. Remarkably, compound **22** decreased only the levels of BNip3 (Figure 4D) without affecting the expression of Ang-2 (Figure 4E). These results provide further support for the specific involvement of HIF-1α in the effects induced by compound **22**. In addition, and to discard potential effects of this derivative upstream of HIFs, we verified that compound **22** did not affect the expression levels either of HIF-1α or of HIF-2α (Figure 4F).

Antiangiogenic Gene Profile of Hypoxic MCF7 Cells Treated with Compound 22. To further confirm the antiangiogenic profile of compound **22**, we analyzed the expression of 84 key genes involved in angiogenesis in hypoxic MCF-7 cells treated with this compound. We identified 12 genes that were significantly affected by compound **22** (fold change $\geq$ 2; Figure 5). As expected, several proangiogenic genes were downregulated in the presence of compound **22**. Among them are several cytokines such as CCL11, IL-1β, or the chemokine-like PROK2 that have been linked to angiogenesis in solid tumors[22−24] as well as other known

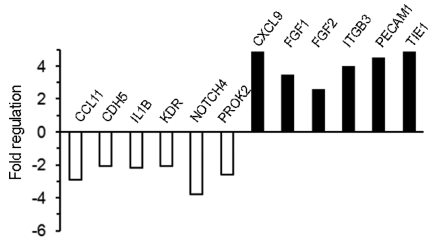

Figure 5. Compound **22** regulates the expression of angiogenesis-related genes. An angiogenesis PCR array was performed in hypoxic MCF7 cells challenged with compound **22** or the corresponding vehicle. The graph shows the 12 genes that were modulated (threshold = 2-fold increase/decrease) in compound **22**-treated cells vs control cells. Results are expressed as fold regulation.

DOI: 10.1021/jm5019252
J. Med. Chem. 2015, 58, 3757−3766

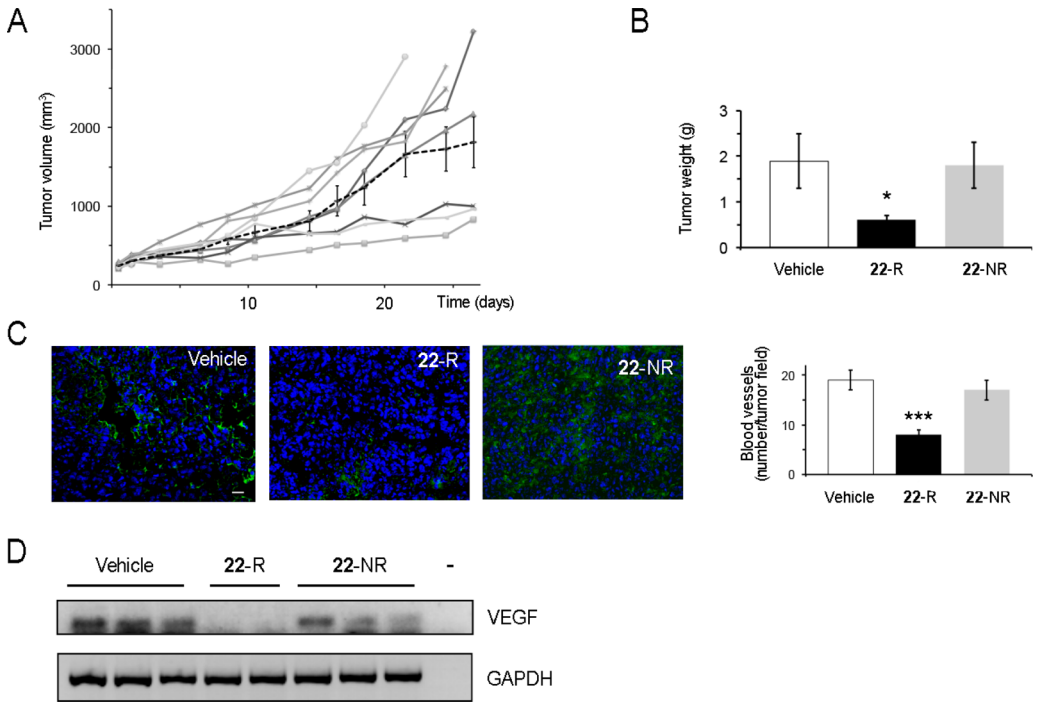

Figure 6. Antitumor effects of compound **22** in a breast cancer xenograft model. (A) Tumor growth in vehicle-treated (represented as mean ± SEM, gray dashed line, $n = 8$) and compound **22**-treated animals (represented individually, $n = 8$, solid gray lines). (B) Tumor weight at the end of the treatment for vehicle-treated animals (white bar), compound **22**-responding animals (black bar), and compound **22**-treated not-responding animals (gray bar). (C) Compound **22** significantly reduces angiogenesis in responding animals (**22**-R), whereas it does not affect the number of blood vessels in treated but not-responding animals (**22**-NR). Images correspond to representative immunofluorescence stainings of tumor sections of each experimental group. Blood vessels are stained with an antibody against CD31 (in green), and nuclei are shown in blue. Scale bar, 100 μm. The bar graph represents the number of blood vessels (mean ± SEM, 3 tumors/experimental group and 4 sections/tumor) for vehicle-treated animals (white bar), compound **22**-responding animals (black bar), and not-responding animals (gray bar). *, $P < 0.05$; ***, $P < 0.001$ (vs compound **22**-treated nonresponding mice) (Student's t test). (D) Compound **22** significantly reduces VEGF mRNA levels in responding animals (**22**-R) compared to vehicle-treated mice or mice treated with compound **22** that are not responding (**22**-NR). Images correspond to representative data obtained from independent samples of tumor sections from each experimental group. Controls include lack of RNA (right lane, labeled −) and GAPDH as housekeeping gene.

proangiogenic factors such as the vascular endothelial cadherin CDH5 and the receptors VEGFR-2 (also known as KDR) and Notch4.[25] On the other hand, upregulation of several genes in response to compound **22** was also observed, including the chemokine CXCL9, which has been described as attenuating angiogenesis in some situations.[26] Surprisingly, we observed an increase in the transcript levels of certain proangiogenic factors such as the cell adhesion molecules integrin ITGB3 and PECAM1, the angiopoietin receptor TIE1, and the proangiogenic factors FGF1 and FGF2. These apparently contradictory results may be due to differential regulation at the transcriptional and translational levels. In this regard, for example, it is worth noting that although some increase is observed at the transcriptional level (Figure 5) compound **22** reduces the protein levels of FGF2 (bFGF), as shown in Figure 2B.

Antitumor Effect of Compound 22 in Vivo. In order to assess the in vivo efficacy of compound **22**, we used a breast cancer xenograft model. Tumor-bearing mice were injected intraperitoneally with compound **22** (25 mg/kg) once a day for 28 days, and tumor volumes were routinely measured (Figure 6A). In vehicle-treated animals, tumors grew in an exponential manner. Treatment of mice with compound **22** produced no effect in 62% of them (5 out of 8), but we observed a significant reduction in tumor growth (ranging from 46 to 55%) in the remaining 38% (3 out of 8) (Figure 6B).

To analyze the in vivo inhibition of angiogenesis, we quantified the number of blood vessels within the tumors by immunofluorescence staining of CD31 (a marker of endothelial cells) in vehicle-treated animals as well as in responding and not-responding individuals (Figure 6C). Significant inhibition of angiogenesis was not detected in nonresponding animals. In contrast, in the tumors of compound-responding mice, a marked reduction in the number of blood vessels was observed. Remarkably, this result correlates with the expression level of VEGF (Figure 6D). Importantly, the inhibition of angiogenesis and tumor growth induced by compound **22** was not accompanied by any sign of toxicity, as assessed by histopathological analysis of liver, lungs, spleen, and heart of compound-treated animals (data not shown). The degree of interindividual variability in the response to **22** might be related to a different bioavailability of the compound caused by the distinct growth and size of each individual tumor or by the existence of clonal variability of xenograft cells, something that has been previously observed for other antitumor targets[27] and also in the clinic after treatment with other angiogenesis inhibitors. In this case, it is possible that increasing the number of individuals would also augment the number of positive cases. In addition, it is important to note that a tumor is a heterogeneous entity, with hypoxic portions but also with other zones, near the blood vessel, which are not hypoxic, and each may have different signaling factors. In this context, Figure

DOI: 10.1021/jm5019252
J. Med. Chem. 2015, 58, 3757−3766

5 suggests upregulation of some proangiogenic genes even in the presence of compound **22**. Hence, it is possible that in the mice in which the drug decreased tumor size the effects of the downregulated proangiogenic genes predominated, whereas the increase in tumor size observed in the other mice was dominated by effects of the proangiogenic genes that remained upregulated even in the presence of the compound.

In conclusion, in this work, we describe a new series of antiangiogenic compounds. Among them, the optimal compound (**22**) inhibits proangiogenic signaling under hypoxic conditions in breast cancer cells. Specifically, administration of **22** decreases the levels of the proangiogenic molecules VEGF, bFGF, and NO. Also, this compound inhibits the active forms of the corresponding receptors of these factors (phosphorylated forms of VEGFR and bFGFR) and the levels of the iNOS enzyme. These effects correlate with a blockade of the MAPK pathway and the inhibition of cellular migration, and they are mediated by HIF-1α, since the effects of compound **22** mostly disappear when its expression is knocked-down. Additionally, gene profiling identified a set of genes related to angiogenesis whose expression is altered by compound **22** and that might contribute to the antiangiogenic effects. Furthermore, administration of compound **22** in a xenograft model produced tumor growth reductions ranging from 46 to 55% in the 38% of the treated animals. Importantly, in the responding tumors, a significant reduction in the number of blood vessels and in the levels of VEGF was observed, further supporting the mechanism of action of the compound. Although better efficacy would be desirable, the fact that compound **22** did not induce any toxic effects in vivo and that it was able to effectively block angiogenesis in the tumors of responding animals strongly support the potential of this compound as a lead for the development of new antiangiogenic agents suitable for the treatment of cancer either alone or in combination with other benchmark drugs.

EXPERIMENTAL PROCEDURES

Compound Synthesis. Unless stated otherwise, starting materials, reagents, and solvents were purchased as high-grade commercial products from Sigma-Aldrich, Acros, ABCR, Bachem, Fluorochem, Scharlab, or Panreac and were used without further purification. Dichloromethane was freshly distilled from calcium hydride. Tetrahydrofuran and diethyl ether were freshly distilled from sodium and benzophenone. All nonaqueous reactions were performed under an argon atmosphere in oven-dried glassware. Full details regarding the synthetic procedures and characterization data of all compounds are given in the Supporting Information. Spectroscopic data of all described compounds were consistent with the proposed structures. Satisfactory HPLC chromatograms and elemental analyses (C, H, N) were obtained for the final compounds, confirming a purity of at least 95% for all tested compounds. Pharmacokinetic properties of selected compounds **3**, **7**, **8**, **21**, and **22** were determined at CEREP (www.cerep.fr).

The synthesis and structural characterization of derivative **22** is detailed below. Detailed procedures and structural data for the rest of the compounds can be found in the Supporting Information.

Synthesis of 2-Hydroxy-5-({[methyl(phenyl)amino]carbonyl}oxy)benzoic Acid (28). To a solution of benzyl ester **14** (120 mg, 0.3 mmol) in absolute EtOH (20 mL) was added 10% Pd/C (50 mg), and the mixture was hydrogenated at room temperature for 4 h, with an initial hydrogen pressure of 30 psi. The reaction mixture was filtered through a pad of Celite and washed with EtOH. The solvent was evaporated to afford the title pure compound as a solid in quantitative yield. mp 157−158 °C. R_f (dichloromethane/EtOH, 95:5) 0.20. IR (KBr, cm^{-1}) 3071, 1699, 1596, 1489. ^{1}H NMR ($CDCl_3$) δ 3.44 (s, 3H), 6.95 (d, 1H, J = 8.9), 7.22−7.45 (m, 6H), 7.61 (m, 1H). ^{13}C NMR ($CDCl_3$) δ 38.4 (CH_3), 114.2 (C), 118.8, 119.1, 126.1, 127.0, 127.3 (5CH), 129.3 (3CH), 142.5, 142.7, 154.8, 159.2, 169.8 (5C).

Synthesis of 4-Hydroxy-3-{[(pyridin-3-ylmethyl)amino]carbonyl}phenyl methyl(phenyl)carbamate (22). To a solution of benzoic acid **28** (228 mg, 0.8 mmol) in anhydrous DMF (10 mL) were added EDC (230 mg, 1.2 mmol) and DMAP (23 mg, 0.3 mmol), and the mixture was stirred at room temperature for 15 min. Then, a solution of pyridin-3-ylmethylamine (87 mg, 0.8 mmol) in DMF (5 mL) was added at 0 °C, and the reaction mixture was stirred for 2 h at this temperature and at room temperature for 14 additional hours. The mixture was evaporated, and the residue was purified by column chromatography (dichloromethane/EtOH, 95:5) to give compound **22** in 37% yield. mp 110−112 °C. R_f (dichloromethane/EtOH, 9:1) 0.32. IR (KBr, cm^{-1}) 3348, 1719, 1646, 1599, 1545, 1492. ^{1}H NMR ($CDCl_3$) δ 3.35 (s, 3H), 4.40 (d, 2H, J = 5.7), 6.87 (d, 1H, J = 9.0), 7.04−7.06 (m, 1H), 7.19−7.36 (m, 6H), 7.41 (m, 1H), 7.60 (d, 1H, J = 7.9), 8.12 (m, 1H), 8.44 (br s, 2H). ^{13}C NMR ($CDCl_3$) δ 38.7 (CH_3), 41.3 (CH_2), 115.0 (C), 119.1, 120.2, 124.1, 126.3, 127.2, 127.8 (6CH), 129.5 (3CH), 134.3 (C), 136.5 (CH), 142.9, 143.0 (2C), 148.8, 149.3 (2CH), 154.9, 159.0, 169.4 (3C).

Inhibition of bFGF-Induced Cell Proliferation of Human Umbilical Vein Endothelial Cells (HUVECs). HUVECs, obtained from American Type Culture Collection, were cultured in a humidified atmosphere of 95% air and 5% CO_2 at 37 °C in M199 medium containing 10% fetal bovine serum (FBS) and 10 μg/mL heparin. Cells were incubated in the presence of bFGF (1 μg/mL) and the appropriate concentration of compound or vehicle (0.4% DMSO) for 2 days, and cell proliferation was quantified spectrofluorimetrically. IC_{50} values are the mean from at least two independent experiments carried out in triplicate. In all cases, the standard error of the mean (SEM) is within 10% of the mean value.

Determination of VEGF and bFGF Levels. Cells were seeded in 12-well plates at a density of 5×10^4 cells per well and were grown for 24 h to obtain a 70−80% confluent monolayer. Then, medium was replaced with fresh DMEM with or without 150 μM $CoCl_2$. After 5 h, compound **22** or vehicle (DMSO) was added to the culture medium, and cells were incubated for 4 h more. Supernatants were then collected and used straightaway or stored at −80 °C for further use. Concentrations of VEGF and bFGF in the culture medium were measured using an enzyme-linked immunosorbent assay (ELISA), according to the manufacturer's instructions (VEGF human ELISA kit and FGF-basic human ELISA kit, Invitrogen). Absorbance was measured at 450 nm using an Asys UVM 340 (Biochrom Ltd., Cambridge, UK) microplate reader, and data were normalized to the kit controls and the number of producing cells. Data from three to five independent experiments carried out in triplicate were represented as mean fold ± SEM with bar graphs.

Nitric Oxide (NO) Quantification. Nitric oxide production was measured through determination of nitrite concentration in the culture medium using the Griess test. Briefly, cells were seeded in 96-well plates at a density of 1×10^4 cells per well in DMEM with 10% fetal bovine serum (FBS) and incubated for 24 h prior to treatments. The medium was then replaced with fresh DMEM with or without 150 μM $CoCl_2$; after 5 h of incubation, compound **22** or vehicle was added, and incubation was continued for another 4 h. Then, 100 μL of supernatant from each condition was mixed with 100 μL of Griess reagent (1% sulphanilamide, 0.1% *N*-(1-naphthyl)ethylendiamine dihydrochloride, 2.5% phosphoric acid). After 15 min at room temperature in the dark, absorbance was measured at 548 nm in an Asys UVM 340 (Biochrom Ltd., Cambridge, UK) microplate reader. The concentration of nitrite, a stable oxidized derivative of NO in cultured cells, was determined from a sodium nitrite ($NaNO_2$, Sigma-Aldrich) standard curve. Data from three independent experiments performed in triplicate were presented as mean ± SEM.

Western Blot Analysis. MCF-7 cells were plated at a density of 2×10^6 cells in 15 cm dishes and allowed to grow for 24 h in DMEM with 1% FBS to obtain an 80% confluent monolayer. The medium was then replaced by fresh DMEM with or without 150 μM $CoCl_2$, and cells were incubated for 5 h to allow a hypoxic response to be

DOI: 10.1021/jm5019252
J. Med. Chem. 2015, 58, 3757−3766

generated. After that, compound **22** or vehicle was added, and cells were incubated for 4 h. Cells were washed with PBS and lysed with ice-cold RIPA buffer (50 mM Tris-HCl, pH 7.4, 150 mM NaCl, 1% Igepal) containing protease and phosphatase inhibitors (Roche and Sigma-Aldrich, respectively). Lysates were clarified by centrifugation at 10 000*g* for 10 min at 4 °C and used straightaway or stored at −80 °C until use. Protein concentration was measured (DC protein assay kit, Bio-Rad), and samples with equal amounts of total protein were diluted into Laemmli reducing sample buffer (Bio-Rad) and denatured at 95 °C for 5 min. Samples were then resolved on 4−20% SDS-PAGE gels (Bio-Rad), and proteins were transferred to nitrocellulose membranes (GE Healthcare, Amersham). After 1 h of incubation in blocking buffer [10 mM Tris-HCl, pH 8.0, 150 mM NaCl, 0.05% Tween-20 (TBS-T) with 1% BSA], membranes were incubated overnight at 4 °C with the corresponding primary antibody. Then, membranes were washed three times (5 min each) with TBS-T and incubated with the corresponding secondary antibody for 1 h at room temperature. Protein bands were visualized using enhanced chemiluminescence detection reagents (GE Healthcare, Amersham) in a Fujifilm LAS-3000 developer (Tokyo, Japan) and quantified by densitometry using ImageJ software (NIH).

Primary antibodies were from Cell Signaling and used at a 1:1000 dilution (rabbit anti-phospho-AKT (pS473), rabbit anti-AKT, rabbit anti-phospho-ERK1/2, rabbit anti-ERK1/2, rabbit anti-phospho-MEK1/2, rabbit anti-MEK1/2, rabbit anti-VEGFR, rabbit anti-phospho-VEGFR, rabbit anti-FGFR, and rabbit anti-phospho-FGFR) or from Santa Cruz Biotechnology and used at a 1:200 dilution (mouse anti-HIF-1α, mouse anti-HIF-2α, mouse anti-iNOS, and rabbit anti-β actin). Secondary antibodies used were goat anti-mouse or goat anti-rabbit IgG HRP conjugates (1:5000, Sigma-Aldrich) accordingly. Relative phosphorylation levels from three independent experiments were presented as the mean ± SEM with bar graphs.

Migration or Wound Healing Assay. Cells were seeded in 96-well plates at a density of 1.5×10^5 cells per well in DMEM with 10% FBS and grown for 24 h at 37 °C and 5% of CO_2 to obtain a 90−100% confluent monolayer. Wounds were made with a sterile p20 pipet tip, and each well was washed twice with PBS to eliminate nonadherent cells and cell debris. Fresh DMEM with or without 150 μM $CoCl_2$ was then added, and after 5 h of incubation, compound **22** (50 μM) or vehicle was added. At this time (0 h) and after 48 h, cells were photographed under phase contrast with an Olympus FW1200 microscope. Empty area in each wound was quantified using ImageJ software (NIH) and compared with the corresponding area of the initial wound. The percentage of area from three independent experiments performed in triplicate was presented as the mean ± SEM with bar graphs.

RNA Interference-Mediated Silencing of the HIF-1α Gene. Cells were transfected with specific siRNA duplexes using DharmaFECT 1 as the transfection reagent according to the manufacturer's instructions (Dharmacon-Thermo Scientific, Lafayette, CO). Selective siRNA against human HIF-1α was a smart pool from Dharmacon-Thermo Scientific, and the sequences were as follows: 5′-GAACAAAUACAUGGGAUUA-3′; 5′-AGAAUGAAGUGUACCCUAA-3′; 5′-GAUGGAAGCACUAGACAAA-3′; and 5′-CAAGUAGCCUCUUUGACAA-3′. The nontargeted control sequence, 5′-UUCUCCGAACGUGUCACGU-3′, was from Applied Biosystems-Ambion (Austin, TX). Twenty-four hours after transfection, cells were seeded for ELISA assays, which were performed as described below.

Quantitive Polymerase Chain Reaction (qPCR). RNA from cell cultures or tumor tissues was isolated with TRIzol reagent (Sigma). cDNA was subsequently obtained with Transcriptor reverse transcriptase (Roche). Real-time quantitative PCR assays were performed using the FastStart master mix with Rox (Roche), and probes were obtained from the Universal Probe Library (Roche). The primers used for human HIF-1α were as follows: sense, 5′-GATAGCAAGACTTTCCTCAGTCG-3′; and antisense, 5′-TGGCTCATATCCCATCAATTC-3′. Amplifications were run in a 7900 HT-fast real-time PCR system (Applied Biosystems). Each value was normalized to human β-actin RNA levels as an internal control: sense, 5′-CCAACCGCGAGAAGATGA-3′; and antisense, 5′-CCAGAGGCGTACAGGGATAG-3′.

Gene Expresssion Analysis. The RT^2 profiler PCR array of human angiogenesis (Qiagen, Valencia, CA), which analyzes the expression of 84 key genes involved in modulating the biological processes of angiogenesis, was used. RNA from cell cultures was isolated with TRIzol reagent (Sigma, St. Louis, MO), including a DNA digestion step with genomic DNA elimination mix (Qiagen). cDNA was subsequently obtained with a RT^2 first strand kit according to the manufacturer's instructions (Qiagen). Real-time PCR assay was performed using the RT^2 profiler PCR array of human angiogenesis in combination with RT^2 SYBR Green master mix (Qiagen). Amplifications were run in a 7900 HT-fast real-time PCR system (Applied Biosystems, Carlsbard, CA), and data were analyzed using the SABiosciences PCR array data analysis template Excel (Qiagen).

VEGF Expression Analysis. RNA was isolated from tumors with TRIzol reagent (Invitrogen, Barcelona, Spain) with the real star kit (Durviz, Valencia, Spain), and cDNA was obtained with Transcriptor reverse transcriptase (Roche Applied Science, Barcelona, Spain). The primers used for VEGF-A amplification were as follows: sense, 5′-GTCCTGTGTGCCGCTGAT-3′; antisense, 5′-AGGTTTGATCCGCATGATCT-3′. GAPDH was used as reference (sense, 5′-GGGAAGCTCACTGGCATGGCCTTCC-3′; antisense, 5′-CATGTGGGCCATGAGGTCCACCAC-3′).

Subcutaneous Xenografts. All procedures involving animals were performed with the approval of the Complutense University Animal Experimentation Committee in compliance with European official regulations. Five million MDA-MB-231 breast cancer cells in 100 μL of PBS were subcutaneously injected into the flank of 6-week-old athymic mice (Harlan Interfauna Iberica, Barcelona, Spain). Tumors were routinely measured with an external caliper, and volume was calculated as $(4\pi/3) \times (\text{width}/2)^2 \times (\text{length}/2)$. When tumors reached ca. 200 mm^3, the mice were treated intraperitoneally three times a week with compound **22** (25 mg/kg) or vehicle (DMSO 0.2 mg/μL in PBS) for 4 weeks. After treatment, animals were sacrificed, and tumors and organs were collected. Tumors were divided into different portions for preparation of tissue sections for immunofluorescent staining [frozen in Tissue-Tek (Sakura Finetek Europe, Zoeterwoude, The Netherlands)] or snap frozen for RNA extraction (and stored at −80 °C until use). Organs collected were fixed in formaldehyde and stained with hematoxylin−eosin for analysis.

For immunofluorescence analysis, Tissue-Tek frozen sections were fixed in PFA 4% and were subjected to heat-induced antigen retrieval in citrate buffer. Then, sections were blocked with PBS containing 0.25% TritonX-100 and 10% goat serum and incubated with anti-CD31 (Pharmingen/BD Biosciences, San Jose, CA). Secondary anti-mouse antibodies conjugated with Alexa Flour 488 were from Invitrogen (Carlsbad, CA). Cell nuclei were stained with DAPI (Invitrogen). Images were acquired using a Leica DM400B microscope (Leica, Wetzlar, Germany).

■ ASSOCIATED CONTENT

Ⓢ Supporting Information

Cell migration impairment of compound **22** (Figure S1), detailed synthetic procedures, characterization data of final compounds **1**−**21** and **23**, and intermediates **24**−**26** and **27d**,**e**, and elemental and HPLC-MS purity analyses of final compounds **1**−**23**. The Supporting Information is available free of charge on the ACS Publications website at DOI: 10.1021/jm5019252.

■ AUTHOR INFORMATION

Corresponding Authors

*(M.M.-F.) Phone: 34-91-3944894; Fax: 34-91-3944103; E-mail: marfont@opt.ucm.es.
*(M.L.L.-R.) Phone: 34-91-3944239; Fax: 34-91-3944103; E-mail: mluzlr@quim.ucm.es.

DOI: 10.1021/jm5019252
J. Med. Chem. 2015, 58, 3757−3766

Author Contributions

◆N.I.M.-R. and D.A. contributed equally to this work.

Notes

The authors declare no competing financial interest.

■ ACKNOWLEDGMENTS

This work was supported by Italfarmaco and grants from the Spanish Ministerio de Economía y Competitividad (MINECO, SAF2010-22198, SAF2013-48271, and predoctoral fellowships to F.J.O.-N., M.B., and S.B.-B.), Instituto de Salud Carlos III (PI11/00295 and PI14/01101), and Comunidad de Madrid (S2010/BMD-2353). E.P.-G. is a recipient of a postdoctoral research contract of the Asociación Española Contra el Cáncer. The authors thank Campus de Excelencia CEI Moncloa for a predoctoral fellowship to N.I.M.-R and UCM's CAI Cytometry and Fluorescence Microscopy facility for their assistance.

■ ABBREVIATIONS USED

bFGF, basic FGF; CSI, chlorosulfonylisocyanate; DIEA, *N*,*N*-diisopropylethylamine; EDC, ethyl-3-(3-(dimethylamino)-propyl)carbodiimide; FBS, fetal bovine serum; FGFR, FGF receptor; HIF-1α, hypoxia-inducible factor-1α; HUVECs, human umbilical vein endothelial cells; SEM, standard error of the mean; siRNA, small interfering RNA; VEGF, vascular endothelial growth factor

■ REFERENCES

(1) Ferrara, N.; Hillan, K. J.; Gerber, H. P.; Novotny, W. Discovery and development of bevacizumab, an anti-VEGF antibody for treating cancer. *Nat. Rev. Drug Discovery* **2004**, *3*, 391−400.

(2) Folkman, J. Angiogenesis: an organizing principle for drug discovery? *Nat. Rev. Drug Discovery* **2007**, *6*, 273−286.

(3) Gacche, R. N.; Meshram, R. J. Angiogenic factors as potential drug target: efficacy and limitations of anti-angiogenic therapy. *Biochim. Biophys. Acta* **2014**, *1846*, 161−179.

(4) Wu, J. M.; Staton, C. A. Anti-angiogenic drug discovery: lessons from the past and thoughts for the future. *Expert Opin. Drug Discovery* **2012**, *7*, 723−743.

(5) Bellou, S.; Pentheroudakis, G.; Murphy, C.; Fotsis, T. Anti-angiogenesis in cancer therapy: hercules and hydra. *Cancer Lett.* **2013**, *338*, 219−228.

(6) Helfrich, I.; Scheffrahn, I.; Bartling, S.; Weis, J.; von Felbert, V.; Middleton, M.; Kato, M.; Ergun, S.; Augustin, H. G.; Schadendorf, D. Resistance to antiangiogenic therapy is directed by vascular phenotype, vessel stabilization, and maturation in malignant melanoma. *J. Exp. Med.* **2010**, *207*, 491−503.

(7) Petrillo, M.; Scambia, G.; Ferrandina, G. Novel targets for VEGF-independent anti-angiogenic drugs. *Expert Opin. Invest. Drugs* **2012**, *21*, 451−472.

(8) Turner, N.; Grose, R. Fibroblast growth factor signalling: from development to cancer. *Nat. Rev. Cancer* **2010**, *10*, 116−129.

(9) Lieu, C.; Heymach, J.; Overman, M.; Tran, H.; Kopetz, S. Beyond VEGF: inhibition of the fibroblast growth factor pathway and antiangiogenesis. *Clin. Cancer Res.* **2011**, *17*, 6130−6139.

(10) Liang, G.; Chen, G.; Wei, X.; Zhao, Y.; Li, X. Small molecule inhibition of fibroblast growth factor receptors in cancer. *Cytokine Growth Factor Rev.* **2013**, *24*, 467−475.

(11) Dieci, M. V.; Arnedos, M.; Andre, F.; Soria, J. C. Fibroblast growth factor receptor inhibitors as a cancer treatment: from a biologic rationale to medical perspectives. *Cancer Discovery* **2013**, *3*, 264−279.

(12) Bono, F.; De Smet, F.; Herbert, C.; De Bock, K.; Georgiadou, M.; Fons, P.; Tjwa, M.; Alcouffe, C.; Ny, A.; Bianciotto, M.; Jonckx, B.; Murakami, M.; Lanahan, A. A.; Michielsen, C.; Sibrac, D.; Dol-Gleizes, F.; Mazzone, M.; Zacchigna, S.; Herault, J. P.; Fischer, C.; Rigon, P.; Ruiz de Almodovar, C.; Claes, F.; Blanc, I.; Poesen, K.; Zhang, J.; Segura, I.; Gueguen, G.; Bordes, M. F.; Lambrechts, D.; Broussy, R.; van de Wouwer, M.; Michaux, C.; Shimada, T.; Jean, I.; Blacher, S.; Noel, A.; Motte, P.; Rom, E.; Rakic, J. M.; Katsuma, S.; Schaeffer, P.; Yayon, A.; Van Schepdael, A.; Schwalbe, H.; Gervasio, F. L.; Carmeliet, G.; Rozensky, J.; Dewerchin, M.; Simons, M.; Christopoulos, A.; Herbert, J. M.; Carmeliet, P. Inhibition of tumor angiogenesis and growth by a small-molecule multi-FGF receptor blocker with allosteric properties. *Cancer Cell* **2013**, *23*, 477−488.

(13) Li, D.; Wei, X.; Xie, K.; Chen, K.; Li, J.; Fang, J. A novel decoy receptor fusion protein for FGF-2 potently inhibits tumour growth. *Br. J. Cancer* **2014**, *111*, 68−77.

(14) Wang, Y.; Becker, D. Antisense targeting of basic fibroblast growth factor and fibroblast growth factor receptor-1 in human melanomas blocks intratumoral angiogenesis and tumor growth. *Nat. Med.* **1997**, *3*, 887−893.

(15) Ebos, J. M.; Lee, C. R.; Cruz-Munoz, W.; Bjarnason, G. A.; Christensen, J. G.; Kerbel, R. S. Accelerated metastasis after short-term treatment with a potent inhibitor of tumor angiogenesis. *Cancer Cell* **2009**, *15*, 232−239.

(16) Loges, S.; Mazzone, M.; Hohensinner, P.; Carmeliet, P. Silencing or fueling metastasis with VEGF inhibitors: antiangiogenesis revisited. *Cancer Cell* **2009**, *15*, 167−170.

(17) Paez-Ribes, M.; Allen, E.; Hudock, J.; Takeda, T.; Okuyama, H.; Vinals, F.; Inoue, M.; Bergers, G.; Hanahan, D.; Casanovas, O. Antiangiogenic therapy elicits malignant progression of tumors to increased local invasion and distant metastasis. *Cancer Cell* **2009**, *15*, 220−231.

(18) Semenza, G. L. Hypoxia-inducible factors: mediators of cancer progression and targets for cancer therapy. *Trends Pharmacol. Sci.* **2012**, *33*, 207−214.

(19) Philip, B.; Ito, K.; Moreno-Sanchez, R.; Ralph, S. J. HIF expression and the role of hypoxic microenvironments within primary tumours as protective sites driving cancer stem cell renewal and metastatic progression. *Carcinogenesis* **2013**, *34*, 1699−1707.

(20) Mole, D. R.; Blancher, C.; Copley, R. R.; Pollard, P. J.; Gleadle, J. M.; Ragoussis, J.; Ratcliffe, P. J. Genome-wide association of hypoxia-inducible factor (HIF)-1alpha and HIF-2alpha DNA binding with expression profiling of hypoxia-inducible transcripts. *J. Biol. Chem.* **2009**, *284*, 16767−16775.

(21) Keith, B.; Johnson, R. S.; Simon, M. C. HIF-1α and HIF-2α: sibling rivalry in hypoxic tumour growth and progression. *Nat. Rev. Cancer* **2012**, *12*, 9−22.

(22) Levina, V.; Nolen, B. M.; Marrangoni, A. M.; Cheng, P.; Marks, J. R.; Szczepanski, M. J.; Szajnik, M. E.; Gorelik, E.; Lokshin, A. E. Role of eotaxin-1 signaling in ovarian cancer. *Clin. Cancer Res.* **2009**, *15*, 2647−2656.

(23) Naldini, A.; Filippi, I.; Miglietta, D.; Moschetta, M.; Giavazzi, R.; Carraro, F. Interleukin-1beta regulates the migratory potential of MDAMB231 breast cancer cells through the hypoxia-inducible factor-1alpha. *Eur. J. Cancer* **2010**, *46*, 3400−3408.

(24) Curtis, V. F.; Wang, H.; Yang, P.; McLendon, R. E.; Li, X.; Zhou, Q. Y.; Wang, X. F. A PK2/Bv8/PROK2 antagonist suppresses tumorigenic processes by inhibiting angiogenesis in glioma and blocking myeloid cell infiltration in pancreatic cancer. *PLoS One* **2013**, *8*, e54916.

(25) Leong, K. G.; Karsan, A. Recent insights into the role of Notch signaling in tumorigenesis. *Blood* **2006**, *107*, 2223−2233.

(26) Sahin, H.; Borkham-Kamphorst, E.; Kuppe, C.; Zaldivar, M. M.; Grouls, C.; Al-samman, M.; Nellen, A.; Schmitz, P.; Heinrichs, D.; Berres, M. L.; Doleschel, D.; Scholten, D.; Weiskirchen, R.; Moeller, M. J.; Kiessling, F.; Trautwein, C.; Wasmuth, H. E. Chemokine Cxcl9 attenuates liver fibrosis-associated angiogenesis in mice. *Hepatology* **2012**, *55*, 1610−1619.

(27) Puig, T.; Aguilar, H.; Cufi, S.; Oliveras, G.; Turrado, C.; Ortega-Gutierrez, S.; Benhamu, B.; Lopez-Rodriguez, M. L.; Urruticoechea, A.; Colomer, R. A novel inhibitor of fatty acid synthase shows activity against HER2+ breast cancer xenografts and is active in anti-HER2 drug-resistant cell lines. *Breast Cancer Res.* **2011**, *13*, R131.

DOI: 10.1021/jm5019252
J. Med. Chem. 2015, 58, 3757−3766